



Modeling fines migration and permeability loss caused by low salinity in porous media



Manuel Coronado*, Martín A. Díaz-Viera

Instituto Mexicano del Petróleo, Eje Central Lázaro Cárdenas 152, San Bartolo Atepehuacán, G. A. Madero, Ciudad de México 07730, Mexico

ARTICLE INFO

Keywords:

Low salinity water injection
Fines migration
Fines detachment
Clogging
Permeability loss

ABSTRACT

A new model to describe fines detachment, migration and clogging and the subsequent permeability impairment observed in low-salinity single-phase lab cores flooding experiments is presented. The model takes into account important issues introduced by [Bedrikovetsky et al. \(2010\)](#). In the model we consider two new elements: a modified equation for the attached fines, and a more general mathematical expression for the maximum retention function. The equation describes a smoother kinetics of the attachment-detachment process, and the maximum retention function extends a previous expression to include low critical salinity concentrations. The equation system is solved numerically using the finite element method, and is applied to three published experimental cases of single-phase low salinity water core injection. To this purpose a general model fitting procedure has been developed. It has been found that our model acceptably reproduces the observed behavior of the effective permeability loss and effluent fines production.

1. Introduction

Diverse mechanisms have been proposed along the years to explain the additional oil that can be recovered by low salinity water injection (LSWI) from oil-bearing sandstone formations ([Al-Shalabi and Sepehrnoori, 2016](#); [Sheng, 2014](#)). One of the suggested mechanisms in sandstones has been the detachment and mobilization of fines from the rock surface, due to a salinity reduction of the injection brine, and the subsequent clogging of pore throats that gives place to local permeability impairment. The additional oil is presumably recovered by forcing the injection fluid to get into new flow channels and contact unswept oil from other zones ([Hussain et al., 2013](#); [Zeinjahromi and Bedrikovetsky, 2013](#); [Sheng, 2014](#); [Al-Shalabi and Sepehrnoori, 2016](#)). Multiple laboratory oil-brine core experiments with fines have been conducted to examine the fines effect on LSWI by considering different salinities, fluid injection rates and temperatures ([Sarkar and Sharma, 1990](#); [Fogden et al., 2011](#); [Oliveira et al., 2014](#)). In order to analyze the fines release, migration and clogging process in a simplified fashion, single phase brine injection experiments have been performed ([Lever and Dawe, 1984](#); [Khilar and Fogler, 1984](#); [Hussain et al., 2013](#); [Zeinjahromi et al., 2016](#)) where permeability loss is observed and in some cases correlated to the presence of fines.

An adequate starting work in the modeling of the fines permeability impairment effect and the effluent fines production is to consider a single-phase (brine) system, and then compare the theoretical model

output to the observed experimental results, which is the subject of this paper. We consider (i) the mass balance of the fines classified as: attached, suspended (mobile) and clogging (strained) fines (see [Fig. 1](#)), (ii) a attaching-detaching equation for the fines, and (iii) a growth equation for clogging fines. Further, a relationship between the clogging fines concentration and the permeability is provided.

Models employed come from the deep bed filtration theory and consider the deposition and removal kinetics of the fines on the rock surface and pore throats, as it is well summarized by F. Civan in a recent paper ([Civan, 2016](#)). It is relevant to highlight the work by [Wennberg et al. \(1995\)](#), where a general model for mobilization, migration and clogging of clay particles is presented and a fundamental analysis of the underlying mechanisms is made. In 2011 [Bedrikovetsky et al. \(2010\)](#) provided new ideas to understand and describe the fines processes. Based on experimental evidence and previous works indicating the existence of a critical brine salinity and a critical injection fluid velocity, at which the permeability starts to reduce substantially, they introduce the so called *maximum retention function* or critical retained fines concentration, σ_{cr} . Above this concentration, fines can be released from the rock surface, and below it fines keep attached. This σ_{cr} depends on brine salinity and velocity, thus by reducing salinity or increasing fluid velocity, additional fines are released. These released fines can become strained in the pore throats and hence reduce the permeability. Instead of considering the standard attachment-detachment kinetics of the classical filtration models ([Logan,](#)

* Corresponding author.

E-mail address: mcoronad@imp.mx (M. Coronado).

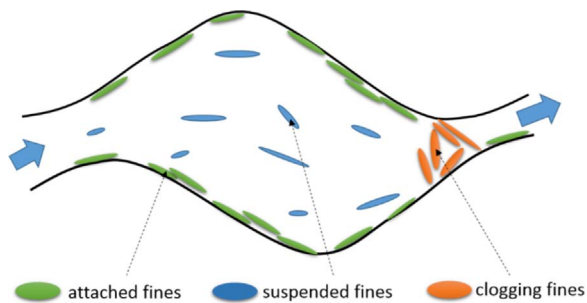


Fig. 1. [Color on-line] Schematic illustration of the fines classification in the interstitial pore space.

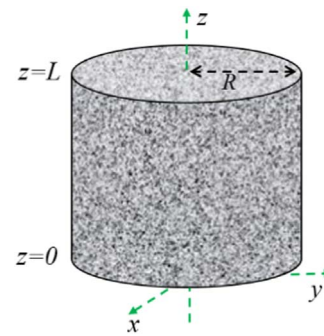


Fig. 2. Core and coordinate system.

2001), Bedrikovetsky et al. propose an abrupt cut-off of the fines detachment process when reaching σ_{cr} . The model can be mathematically written as:

$$\begin{aligned} \partial\sigma_a/\partial t &= -\lambda_d UC_m \quad \text{for } \sigma_a > \sigma_{cr} \\ \sigma_a &= \sigma_{cr} \quad \text{else} \end{aligned} \quad (1)$$

where σ_a is the attached fines concentration (mass/rock volume), C_m is the mobile fines concentration (mass/water volume), λ_d is a detachment rate with dimensions of $length^{-1}$, and U is the fines effective velocity, which will be assume to be the water velocity in which mobile fines are suspended (an assumption that might be questionable (Oliveira et al., 2014)). Further, by performing a torque balance analysis of the involved attaching-detaching forces an expression for σ_{cr} is proposed as (Bedrikovetsky et al., 2010; Zeinijahromi et al., 2012)

$$\sigma_{cr} = \sigma_0 [1 - \epsilon^2] \quad (2)$$

where ϵ is the dimensionless erosion number, which depends on the velocity U , the salinity of the injection brine C_s , the pH and temperature of the brine, etc. (Zeinijahromi et al., 2016). Specifically, it increases with the velocity and reduces with salinity.

In this paper we present a model to describe the effect of fines in low salinity water injection experiments at lab scale based on the work by Bedrikovetsky et al. (2010). The model introduces a modified version of Eqs. (1) and (2). In Eq. (1) the main concept of the maximum (critical) retention concentration is kept, but the physically questionable abrupt cut-off of the attached fines concentration is released. Further, Eq. (2) has been straightforwardly extended to an exponential function to circumvent mathematical problems when considering very low or zero critical salinity concentration, which would imply $\epsilon \gg 1$, and to increase its capacity to adjust experimental results. Finally, we apply the new model to reproduce permeability loss data from three low salinity core injection experiments published in the literature (Lever and Dawe, 1984; Khilar and Fogler, 1984; Zeinijahromi et al., 2016).

2. The mathematical model

The mathematical model considers a cylindrical sandstone core plug of length L and radius R (see Fig. 2), saturated initially with a brine of high salinity. The brine and the rock are assumed to be slightly compressible, with compressibility c_f and c_R respectively. The initial porosity ϕ_0 and permeability k_0 are assumed constant in the core. In the injection experiment the brine is introduced at a constant rate at the inlet face of the core, and kept at constant pressure at the outlet face. Along the time the injection brine salinity is stair-like reduced to a minimum low salinity and the total pressure drop in the core is recorded. The effluent water is periodically collected at the output for fines presence analysis.

The equation system comprehends equations for the fluid pressure p , the brine velocity (Darcy) U , salinity C_s , total fines, attached fines

and clogged fines. Additionally an expression for σ_{cr} in terms of the salinity and an expression for the permeability as function of the clogged fines concentration σ_c should be provided. The partial differential equation system is dynamically coupled, since salinity transport and fines processes involve the advective velocity U , the clogging fines concentration σ_c modifies the permeability, and this in turn affects the pressure.

2.1. Fluid flow

The pressure equation results from the brine mass conservation, the Darcy velocity $\mathbf{U} = -(k/\mu)\nabla p$ and the slightly compressible rock and brine assumption as (Chen et al., 2006)

$$\phi c_T \frac{\partial p}{\partial t} - \nabla \cdot \left[\frac{k}{\mu} \nabla p \right] = 0 \quad (3)$$

where $c_T = c_f + c_R$ is the total compressibility, k the permeability that depends on space and time, and μ the viscosity of the brine. In deriving Eq. (3) also the assumption $c_T(\Delta p)_{max} \ll 1$ was made, being $(\Delta p)_{max}$ the maximum pressure drop. Within this assumption it holds $\phi \sim \phi_0$ and $\rho \sim \rho_0$. Constant porosity means that the volume of effluent fines is negligible in comparison to the core porous volume. In this context, fines inside the core change position by detaching and straining, but keep the total porous volume inside the core essentially constant. The boundary conditions are (i) constant pressure at outlet, $p(x, y, z = L, t) = p_{out}$, (ii) constant volumetric injection rate Q at the inlet, which yields the Neumann condition, $(-k/\mu)(\partial p/\partial z)|_{z=0} = Q/(\pi R^2)$, and (iii) no flow in radial direction of the core. The initial condition is $p(x, y, z, t = 0) = p_0$, and $p_0 = p_{out}$ is further set.

2.2. Salinity transport

The salinity behavior is described by an advective-dispersive equation for the salinity concentration, C_s

$$\phi \frac{\partial C_s}{\partial t} + \nabla \cdot [-D_{L,s} \nabla C_s + \mathbf{U} C_s] = 0 \quad (4)$$

where $D_{L,s} = \alpha_{L,s} U$ is the longitudinal dispersion coefficient of the salt, and the constant $\alpha_{L,s}$ is the corresponding longitudinal dispersivity. The boundary conditions are (i) time-variable salinity at the inlet, $C_s(x, y, z = 0, t) = C_{s,inj}(t)$, (ii) the Danckwerts' condition $(\partial C_s/\partial z)|_{z=L} = 0$ at the outlet, and (iii) no flow in radial direction. The initial condition is $C_s(x, y, z, t = 0) = C_{s,0}$. Further, it is set $C_{s,0} = C_{s,H}$ with $C_{s,H}$ the high salinity concentration. To avoid inconsistencies the injected initial salinity should satisfy $C_{s,inj}(t = 0) = C_{s,H}$.

2.3. Fines transport

The fines dynamics is described by equations involving the three fines types described before. They concern the total fines population mass balance and a model for the attachment-detachment kinetics and

for the clogging process.

2.3.1. Fines balance equation

The balance equation for the fines involves mobile fines dispersion, and the sink-source terms of the attached/detached and strained fines, it is

$$\phi \frac{\partial C_m}{\partial t} + (1 - \phi) \frac{\partial(\chi_f \sigma_a + \sigma_c)}{\partial t} + \nabla \cdot [UC_m - D_{L,f} \nabla C_m] = 0 \quad (5)$$

where σ_a is the attached fines concentration (mass/rock volume), σ_c is the clogging fines concentration (mass/rock volume), $D_{L,f} = \alpha_{L,f} U$ is the longitudinal dispersion coefficient of the mobile fines, $\alpha_{L,f}$ is the longitudinal fines dispersivity, and χ_f is the mass fraction of the rock that can release fines. If fines are entirely associated to clay, then χ_f is the shale fraction in the rock that can provide mobile fines (i.e. the shale fraction exposed to the brine). The boundary conditions are: (i) mobile fines concentration at the inlet, $C_m(x, y, z = 0, t) = C_{m,inj}$, which in our case is set to $C_{m,inj} = 0$ (ii) the Danckwerts' condition $(\partial C_m / \partial z)|_{z=L} = 0$ at the outlet, and (iii) no fines flow in radial direction. The initial condition is $C_m(x, y, z, t = 0) = C_{m0}$. Here, $C_{m0} = 0$ is set.

2.3.2. Attached fines equation

The model we consider is different from the original (Bedrikovetsky et al., 2010) shown in Eq. (1). Here, the existence of the so called maximum retention (critical) attached fines concentration is kept, but the abrupt change in derivative when σ_a is approaching σ_{cr} is changed by a smooth process, which in general might be physically more realistic. For the detachment process ($\sigma_a \geq \sigma_{cr}$) the equation is

$$\frac{\partial \sigma_a}{\partial t} = -\lambda_d U (\sigma_a - \sigma_{cr}) \quad (6)$$

and for the attachment process ($\sigma_a < \sigma_{cr}$)

$$\frac{\partial \sigma_a}{\partial t} = \lambda_a U C_m (1 - \sigma_a / \sigma_{cr}). \quad (7)$$

Here λ_d and λ_a are the detachment and attachment (filtration) coefficient with dimensions $length^{-1}$. $(\lambda_d U)^{-1}$ can be seen as characteristic *delay* time associated to the time the detachment process requires to reach the steady-state $\sigma_a = \sigma_{cr}$. λ_d and λ_a do not necessarily take the same value as in other attaching-detaching models since the equations, although similar, might be different.

It should be mentioned that Eq. (7) has the form of the equations used to describe particle deposition processes, where $(1 - \sigma_a / \sigma_{cr})$ is the *Langmuir blocking function* (Adamczyk, 2003). The maximum retention function σ_{cr} plays the role of the so called maximum jamming coverage and represents the surface saturated state. Further, by considering the dependence of σ_{cr} on the total ion concentration (salinity), the function $\sigma_{cr}(C_s)$ can be seen as an adsorption isotherm.

The initial condition is $\sigma_a(x, y, z, t = 0) = \sigma_{a0}$. The physically maximum value for σ_{a0} can be estimated as (mass of detachable fines)/(rock volume), which in terms of χ_f is

$$\sigma_{a0,max} = \rho_R \chi_f, \quad (8)$$

where ρ_R is the rock density.

2.3.3. Clogging fines equation

The dynamics of the clogging fines is given by the equation

$$\frac{\partial \sigma_c}{\partial t} = \lambda_c U C_m. \quad (9)$$

Here λ_c is a straining coefficient with dimensions $length^{-1}$. The initial condition is $\sigma_c(x, y, z, t = 0) = \sigma_{c0}$. In our case we will assume that at initial time there is some attached fines but no clogging fines present, $\sigma_c = 0$.

2.3.4. Critical attached fines concentration

One of the main new ingredients in the Bedrikovetsky et al.'s model (Bedrikovetsky et al., 2010) is the introduction of the mentioned maximum retention function σ_{cr} that depends on salinity and fines velocity. The expression commonly used is the quadratic form in Eq. (2), where ϵ is a function of fines velocity and brine salinity accordingly to a mechanistic force balance analysis on an attached fines particle, say $\epsilon \sim U/C_s$. When the critical salinity concentration is very small or zero then the case $C_s \rightarrow 0$ can appear implying $\epsilon \rightarrow \infty$. Thus, the expression in Eq. (2) breaks down giving negative values. While showing explicitly only the salinity dependence, we introduce the following new algebraic form

$$\sigma_{cr} = \sigma_{cr0} \exp\{-[C_{s1}/(C_s - C_{s2})]^{nc}\}. \quad (10)$$

Here σ_{cr} has four free parameters $\{\sigma_{cr0}, C_{s1}, C_{s2}, nc\}$. The critical salt concentration (CSC) is slightly larger than C_{s2} . By reducing C_{s1} or increasing nc the fall of the σ_{cr} - curve becomes more abrupt at the CSC. Further, the CSC shifts to larger salinities by increasing C_{s2} . These four parameters might depend on the fluid velocity, temperature and pH as mentioned before. At low salinity ($C_s \rightarrow C_{s2}$) expression (2) is recovered with $\epsilon = C_{s1}/(C_s - C_{s2})$ and $nc=2$. At high salinity ($(C_s - C_{s2}) \gg C_{s1}$) it holds $\sigma_{cr} \rightarrow \sigma_{cr0}$. In general, if we start at a rock-brine equilibrium, it holds $\sigma_{cr0} = \sigma_{a0}$. As we will see below, permeability loss data adjustment require extremely abrupt falls of σ_{cr} at CSC, the original Bedrikovetsky's quadratic dependence could not achieve it.

2.4. Permeability loss

The effect of clogging fines on permeability impairment is described by the damage function (Pang and Sharma, 1997; Hussain et al., 2013)

$$k = k_0 / (1 + \beta \sigma_c) \quad (11)$$

where β is the formation damage coefficient with dimensions $[\sigma_c]^{-1}$.

3. The numerical model

The coupled equation system for fluid flow Eq. (3), salinity transport Eq. (4) and fines dynamics Eqs. (5), (7) and (9) are solved numerically using the finite element method as implemented in Comsol (2008). The Galerkin formulation with quadratic Lagrange polynomials, second-order backwards finite differences time discretization and the Newton-Raphson solver are employed, which gives place to a fully implicit scheme. A grid with uniformly distributed tetrahedral elements was used. In solving the fines attachment-detachment equation a particular numerical convergence problem might appear when switching from the equation for $\sigma_a \geq \sigma_{cr}$ to the equation for $\sigma_a < \sigma_{cr}$ or vice versa. However, since just salinity reduction is here considered, only Eq. (6) appears and therefore to avoid convergence problems we straightforwardly extend its domain to include $\sigma_a < 0$. Further, in order to reduce potential convergence problems, all abrupt changes, as those set on salinity at the inlet, are smoothed by sigmoid functions.

4. Model results: application to core flooding experiments

In this section we apply our model to analyze some low salinity water injection experiments made by Lever and Dawe (1984), Khilar and Fogler (1984) and Zeinijahromi et al. (2016). The experiments consider the injection at constant flow rate in sandstone cores, while the salinity of the injection brine is stair-like reduced and the change in the effective permeability measured as function of the porous volume injected (PVI). The objective of these applications is to examine the model capacity to reproduce and explain the experimentally observed permeability loss and the effluent fines concentration, both as function of PVI. To make this comparison we use the normalized effective

Table 1
Parameters used to reproduce Lever and Dawe experimental data.

Parameter	Value
Core length, L	2.2 cm
Core diameter, D	2.4 cm
Porosity, ϕ	14.37%
Porous volume, PV	1.43 ml
Initial permeability, k_0	140 mD
Water viscosity, μ	1 cP
Water density, ρ	1 g/ml
Total compressibility, c_T	6×10^{-10} 1/Pa
Longitudinal salt and mobile fines dispersivity, $\alpha_{L,s}, \alpha_{L,f}$	$L/10$
Injection rate, Q_{inj}	20 ml/h
Pressure at outlet, p_{out}	1 atm
Rock fraction containing detachable fines, χ_f	8%w
Detaching coefficient, λ_d	7 m^{-1}
Clogging coefficient, λ_c	0.005 m^{-1}
Parameter σ_{cr0} in σ_{cr}	130 g/l
Formation damage coefficient, β	$27,000 \text{ (g/l)}^{-1}$
Parameter C_{s1} in σ_{cr}	0.006049%w
Parameter C_{s2} in σ_{cr}	0.001827%w
Parameter nc in σ_{cr}	1.0366

permeability (Khilar and Fogler, 1984).

$$k_{eff}(t) = (4Q_{inj}L\mu)/[\pi D^2(p(z=0, t) - p_{out})k_0], \quad (12)$$

and the effluent fines concentration $C_f(z=L, t)$. The applications are described below.

4.1. Lever and Dawe experiment

In the core injection experiments by (Lever and Dawe, 1984) some samples from a sandstone formation in Scotland were employed to study the sensitivity of the rock to various brine types. In our work the data corresponding to their NaCl brine injection are examined. The rock samples contain near 90% Quartz and only tracers of Clay minerals, mainly Muscovite and Illite. The pore spaces are reported to have small amounts of fines material (quartz). The core plugs used are 2.2 cm long and have 2.4 cm in diameter, with permeability to dry air and porosity varying from 45 to 120 mD and from 7.1% to 14.6% respectively, giving place to porous volumes between 0.7 and 1.9 ml. The brine salinity has been sequentially reduced from its initial saturation value of 3w% to 2, 1, 0.5, 0.25, 0.125, 0.05, 0.025, 0 w%, each step after a 100 ml stabilization injection period. Lever and Dawe plot their experimental results of permeability and effluent fines concentration as function of volume injected, these are the data

employed in this work. In Table 1 the parameters used to reproduce the experimental data are displayed. The salinity reduction at the core plug inlet as function of the injected volume is plotted in Fig. 3(a). The corresponding PVI is {70, 140, 210, 280, 350, 420, 490, 570}. The last computing time equals $PVI=777$. With $\chi_f = 8\%$ and Eq. (8) the condition $\sigma_{a0} < 187 \text{ g/l}$ should hold. In Fig. 3 (b) the critical (maximum) retention function of attached fines, σ_{cr} , as function of salinity is displayed. It shows almost no change from 3% down to 0.5% salinity, but below this value an abrupt reduction in σ_{cr} occurs. This behavior mimics the existence of the critical salinity value, where below this value a dramatic permeability loss appears.

The pressure behavior as function of the plug length z and PVI is displayed in (Fig. 4). In Fig. 4(a) the pressure as function of PVI evaluated at three positions $z = \{0, L/2, L\}$ and in Fig. 4(b) the pressure as function of z for various PVI are shown. The PVI displayed corresponds to the pressure profile previous to the salinity change, but also the initial and final PVI (i.e. 0 and 777) are here for reference displayed. The increase in the pressure is a consequence of the permeability reduction caused by the clogging fines, as described below. The pressure gradient in z -direction versus z is shown in Fig. 5(a) for various PVI's. The pressure gradient increases with z and with the PVI, as a consequence of the permeability loss due to the effect of the clogging fines. The z -velocity component versus PVI for various z is presented in Fig. 5(b), it increases with z . This can be explained by the increasing permeability loss as moving to the plug end. Lower permeability means smaller effective flow cross section, and in order to keep the total flow constant, the velocity should increase with z .

The dynamics of the salinity is described in (Fig. 6a), where the flooding of the low salinity front along the core length is described at various times. The salinity starts reducing from 3% to 2% at $z=0$ (inlet) and a low-salinity front moves inside the plug. After a short time the salinity temporarily stabilizes and get constant at 2% inside the plug. However, the next step appears at the inlet, and brings salinity to 1%, thus, a second low-salinity front advances inside the plug. This process repeats various times following the stair-like behavior shown in Fig. 3(a). The shape of the salinity decrement seen at the outlet of the plug (not drawn) is fully similar to the decrement appreciated at the inlet in Fig. 3(a), it is just a few porous volume delayed. The salinity decrement front removes attached fines as long as it travels inside the core. The detaching process at the plug inlet is illustrated in Fig. 6(b), where the maximum (critical) retention function σ_{cr} (in red) is given in terms of PVI accordingly to the curve in Eq. (2). The attached fines concentration (green curve) follows it up, and slowly adjust it down to the new σ_{cr} value, until it finally reach zero (fresh water flooding). The released fines become mobile fines, and its concentration as function of

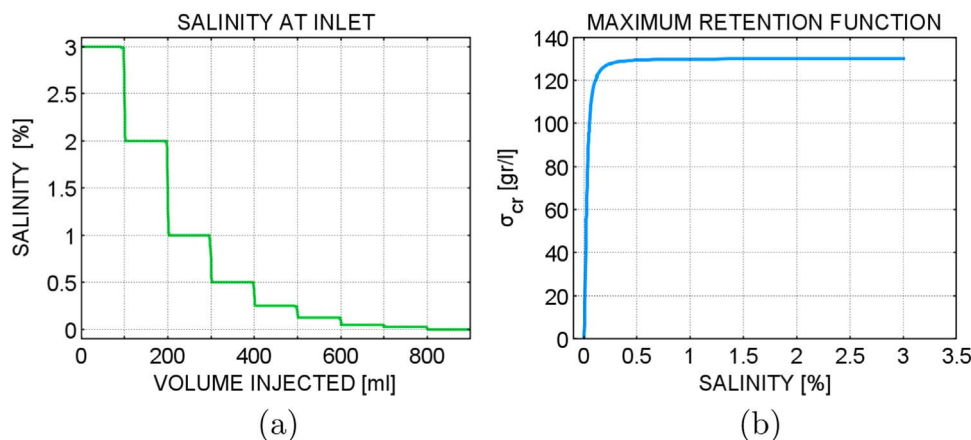


Fig. 3. Lever and Dawe experiment. (a) Salinity at inlet versus volume injected, and (b) Maximum retention function as function of salinity.

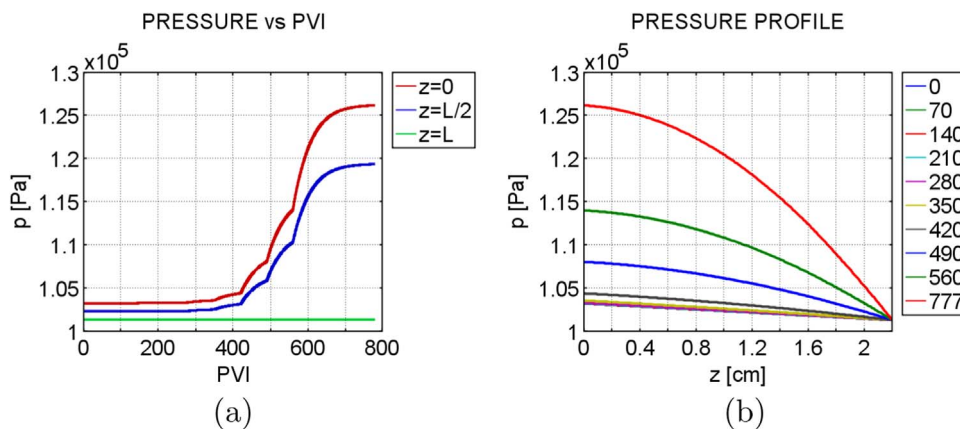


Fig. 4. [Color on-line] Pressure behavior of Lever and Dawe experiment (a) Pressure as function of PVI at three positions $\{z = 0, L/2, L\}$, and (b) pressure as function of z at some PVI's previous to the salinity reduction step, including initial (PVI=0, bottom curve) and final (PVI=777, top curve) profiles.

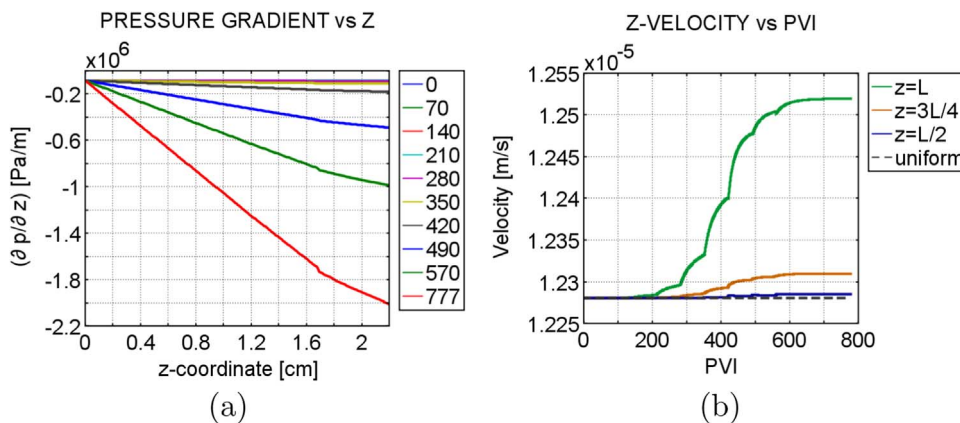


Fig. 5. [Color on-line] (a) Pressure gradient profile of the Lever and Dawe test at various PVI, and (b) Velocity as function of PVI at three positions $\{z = L, 3L/4, L/2\}$, here also the uniform velocity corresponding to the velocity without permeability loss is plotted.

PVI for $z = \{0, L/2, L\}$ is displayed in (Fig. 7a). In this figure various pulses of fines can be observed, which correspond to the low-salinity reduction steps. Accordingly to the behavior illustrated in (Fig. 6b), the last peaks are the largest.

The attached fines behavior is shown in (Fig. 8). Its concentration keeps constant at initial PVI's, and starts reducing at PVI ~ 400 , when the salinity goes below $\sim 0.05\%$ as indicated in (Fig. 3b) and (6b). It is to be observed in (Fig. 8) that the attached fines concentration although reducing in time, it is always almost uniform inside the plug Fig. 9.

The clogging fines behavior is described in (Fig. 9), in (a) its

concentration as function of PVI is shown for three position in the plug, $z = \{0, L/2, L\}$. At the plug input there are not fines clogged, and the amount of clogged fines increase with the distance inside de plug and with time (i.e. PVI). The (Fig. 9b) illustrates the profile of the clogging concentration at times corresponding to the last (and largest) fines release, here PVI between 555 and 595. The profile increases with z almost linearly, except at the end, where the derivative of σ_c becomes zero, since it inherited this from the boundary condition on the salinity and the mobile fines.

The normalized effective permeability, k_{eff} , versus the volume

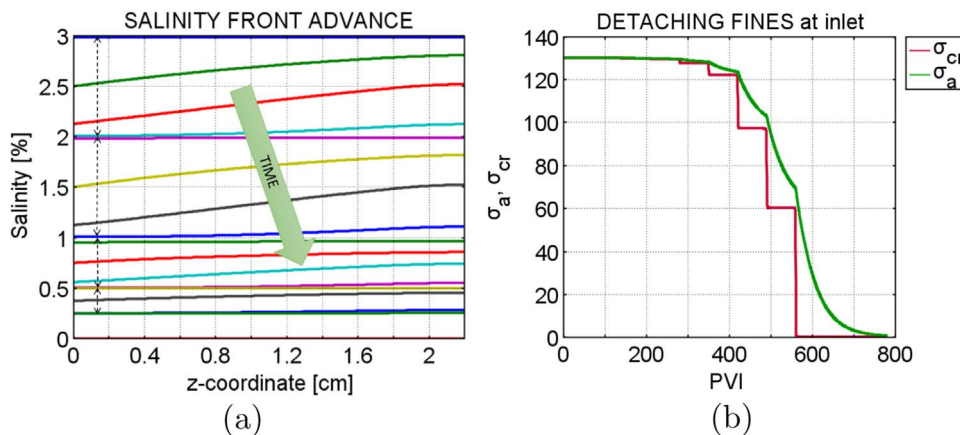


Fig. 6. [Color on-line] (a) Dynamics of the salinity concentration versus z at various times for the first down steps accordingly to (Fig. 3a), and (b) Maximum retention function (σ_{cr} , red curve) and reducing attached fines concentration (σ_a , green curve) at inlet ($z=0$) as function of PVI.

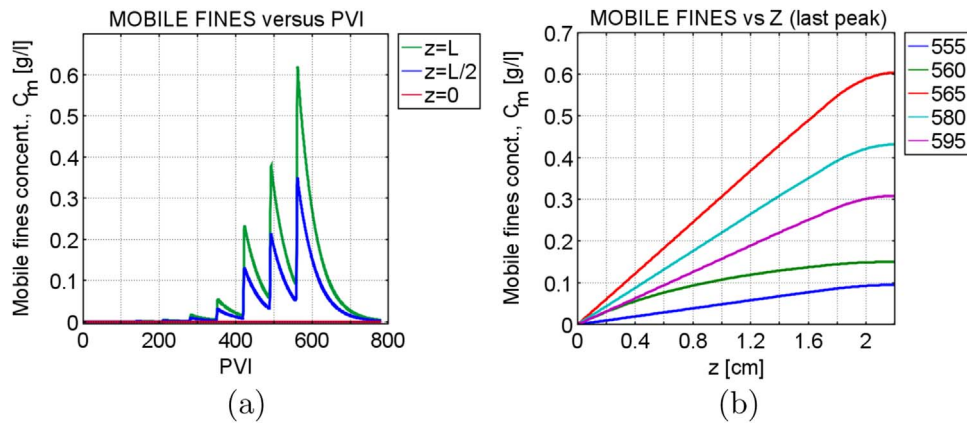


Fig. 7. [Color on-line] (a) Pulses of mobile fines concentration as function of PVI for various z, and (b) mobile fines profile at various PVI around the last peak.

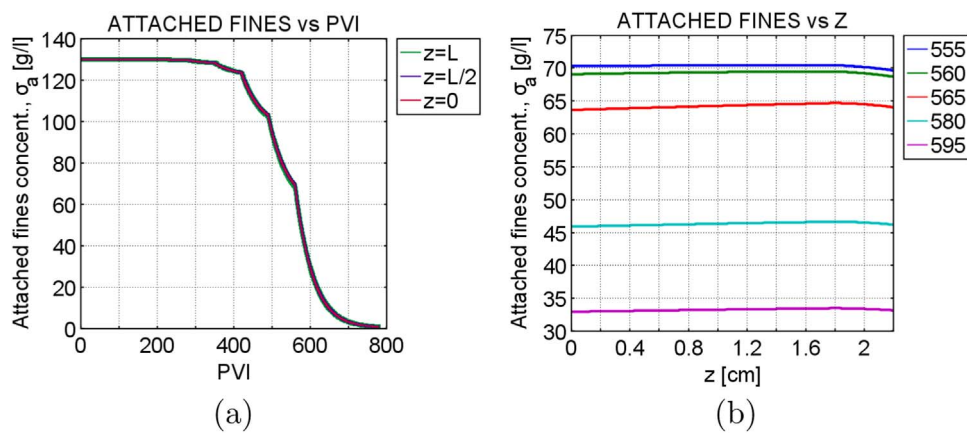


Fig. 8. [Color on-line] (a) Attached fines concentration as function of PVI for various z, and (b) attached fines profile (σ_a vs z) at various PVI corresponding to the last fines detachment peak.

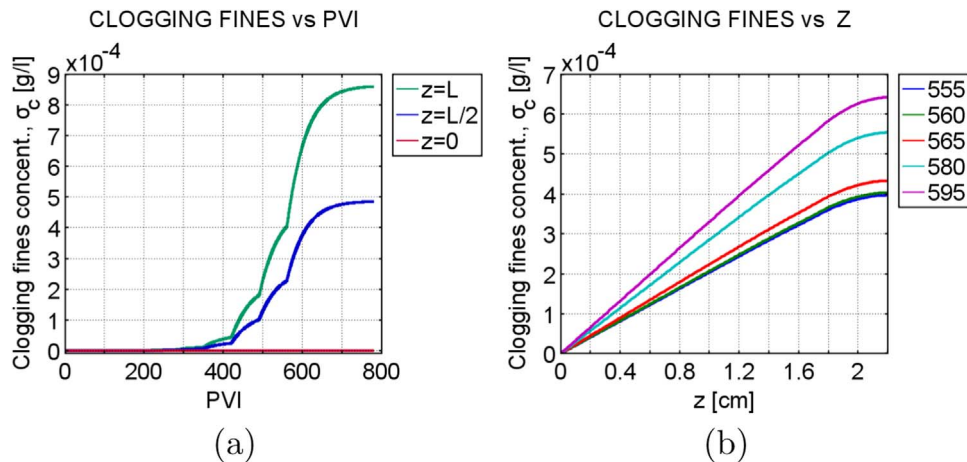


Fig. 9. [Color on-line] (a) Clogging fines concentration as function of PVI for various z, and (b) clogging fines profile (σ_c vs z) at various PVI corresponding to the last peak.

injected is plotted In Fig. 10 (a), in blue the model results and the experimental data as red circles. The fines concentration in the effluent shows various peaks along time (here volume injected, VI) as shown by the blue curve of Fig. 10(b). The peaks are caused by the low-salinity reduction steps. In this figure the effluent fines experimental results are presented as histogram in red lines. These values correspond to the cumulated fines concentration, measured in effluent samples collected during 100 ml. The value shown is thus the average concentration in that period. The procedure developed to simultaneously fit the model to both data series is described in the Appendix and yields the

fitting parameters shown Table 1. The model appropriately describes the general permeability and effluent fines concentration behavior. It marks the correct permeability features position in time, the tendencies and the approximate amount of change. In the plots shown in (Fig. 10) the adjustment of the permeability has been privileged over the effluent fine concentration, However, the overall behavior and total amount of the effluent fines (area below the curve) are well described.

The parameters $\lambda_d = 7 \text{ m}^{-1}$ and $\lambda_c = 0.005 \text{ m}^{-1}$ were used to fit the data as displayed in Table 1. The value λ_c is smaller than the values reported for deep bed filtration and internal cake formation in well

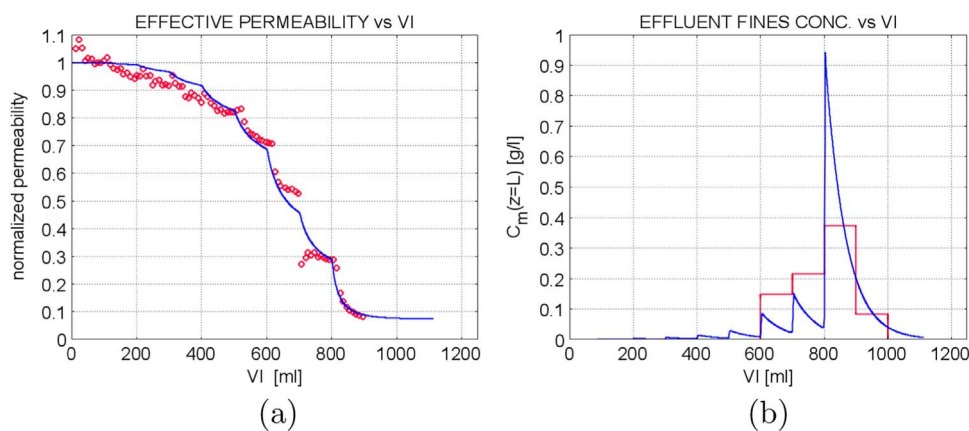


Fig. 10. [Color on-line] Experimental Lever and Dawe data reproduction (a) Permeability model (blue curve) and permeability data (red circles) as function of the fluid volume injected, (b) Effluent fines concentration model (blue line) and data (red lines) as function of volume injected.

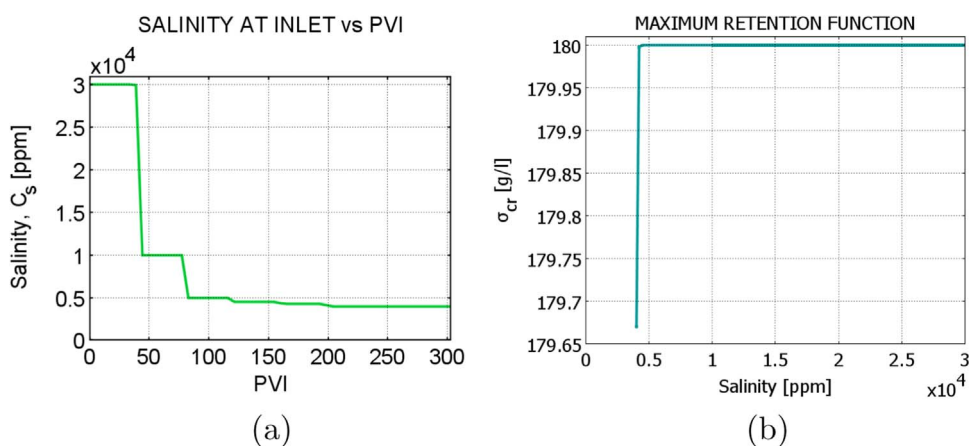


Fig. 11. Khilar and Fogler application: (a) Salinity at inlet versus porous volume injected, and (b) Maximum retention function in terms of salinity.

injectivity decline, where $\lambda \sim 0.1 - 100 \text{ m}^{-1}$ (Pang and Sharma, 1997; Zeinijahromi et al., 2012). The corresponding characteristic length of the detaching and clogging process found here are $\lambda_d^{-1} = 0.14 \text{ m}$ and $\lambda_c^{-1} = 200 \text{ m}$. This means that fines detachment occurs in a relatively short scale length after salinity is reduced, but fines straining occurs in a much longer scale length. This means, fast released fines will travel a long length before getting strained.

4.2. Khilar and Fogler experiment

A second single-phase core flooding experiment analyzed is that reported by (Khilar and Fogler, 1984). Here, a Berea sandstone plug is used to study the effect of the salinity reduction on the fines release and permeability loss. The mineral weight composition of the core is 80% Quartz, 12% Feldspar and 8% dispersible clay (primarily Kaolinite with some Illite). No Montmorillonite swelling clays were detected. In these experiments cores were flooded at constant rate with a brine that reduces its salinity in time. They performed various experiments considering diverse salts and temperatures, and evaluate in each case the critical salt concentration (CSC) at which permeability reduces abruptly. Of our interest is the experiment with a NaCl-brine at 3 °C and $Q_{inj} = 100 \text{ ml/h}$, in which the salinity is decreased stair-like from 30,000 ppm to 10,000, 5000, 4500, 4250, 4000 ppm, with intermediate 40 PVI stabilization periods, as shown in (Fig. 11a). A CSC value is found around 4125 ppm, which yields a permeability loss of 43%. Effluent fluid samples were analyzed finding clay fines (kaolinite with some traces of illite) during the final 4000 ppm injection period. The amount of fines mass collected during $\Delta t = 1 \text{ hour}$ ($\sim 40 \text{ PVI}$) is $M_f = 560 \mu\text{g}$ (Khilar, 1981). Hence, the average fines mass concentra-

tion during this period is $M_f/(Q_{inj} \Delta t) = 5.6 \times 10^{-3} \text{ g/l}$. This experimental value for the effluent fines concentration, and the experimental permeability loss data are employed to tune our model. Accordingly to Eq. (8) it should hold $\sigma_{a0} < 208 \text{ g/l}$. The procedure we developed to adjust our model to experimental results is described in the Appendix. The parameter values used are displayed in Table 2. A good data fitting is achieved as discussed below.

Table 2

Parameters used to reproduce Khilar and Fogler experimental data.

Parameter	Value
Core length, L	2.54 cm
Core diameter, D	2.54 cm
Porosity, ϕ	19.0%
Porous volume, PV	2.44 ml
Initial permeability, k_0	100 mD
Water viscosity, μ	0.3 cP
Water density, ρ	1 g/ml
Total compressibility, c_T	$6 \times 10^{-10} \text{ 1/Pa}$
Longitudinal salt and mobile fines dispersivity, $\alpha_{L,s}, \alpha_{L,f}$	L/10
Injection rate, Q_{inj}	0.027 ml/s
Pressure at outlet, p_{out}	2900 psi
Rock fraction containing detachable fines, χ_f	8%w
Detaching coefficient, λ_d	10 m^{-1}
Clogging coefficient, λ_c	0.5 m^{-1}
Parameter σ_{cr0} in σ_{cr}	180 g/l
Formation damage coefficient, β	7000 (g/l)^{-1}
Parameter C_{s1} in σ_{cr}	18 ppm
Parameter C_{s2} in σ_{cr}	3905.5 ppm
Parameter nc in σ_{cr}	3.8

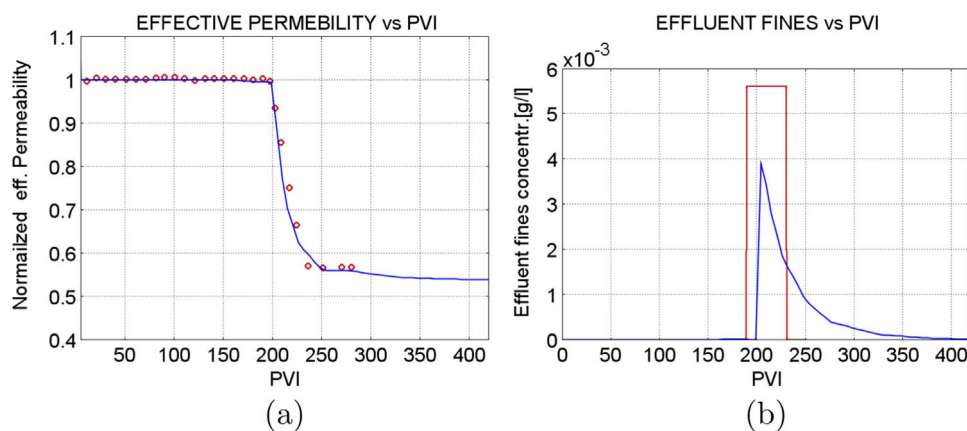


Fig. 12. [Color on-line] Experimental Khilar and Fogler data reproduction: (a) Permeability loss versus PVI, and (b) effluent fines concentration as function of PVI. Data in red and model in blue.

The results are displayed in (Fig. 12), where in plot (a) the normalized effective permeability is shown and in plot (b) the effluent concentration. We can observe that the permeability curve of the model (solid blue line) in Fig. 12(b) reproduces fairly well the data points (red circles). The effluent fines concentration (blue line) has correctly a single peak at around 200 PVI corresponding to the last salinity reduction (close to the CSC). Although the high of the peaks is smaller than the data value (red line histogram), the total area below the model curve and the data curve are similar, what approximately corresponds to the same total fines mass produced.

4.3. Zeinijahromi et al. experiment

A third application of our model has been done to the single-phase core injection experiment in sample #1 reported by Zeinijahromi et al. (2016). In this experiment a Berea sandstone plug of length $L = 17.0$ cm, diameter $D = 4.0$ cm and permeability $k_0 = 76$ mD was used. A NaCl brine flooding was performed at a constant injection rate of 0.1 ml/min. The brine salinity was step-wise reduced from its initial saturation value of 3 wt% to {2, 1, 0.5, 0.25, 0.125, 0.05, 0} wt%, as shown in Fig. 13 (a).

The effective permeability loss and the effluent fines concentration (ppm volume) was measured along the time and reported as function of PVI, as can be seen as red circles in Fig. 14. A low amount of fines were produced in comparison with the two previous applications discussed above, and were essentially produced at the final salinity reduction steps, mainly from 0.05% to fresh water. In a similar fashion, the main permeability loss occurs in this last salinity transition, but a small loss is also seen in a step before, when salinity goes from 0.125% to 0.05%. The large total permeability impairment (~40 folds) seems to correlate

with the highly small amount of fines produced, what can point to a big fines fraction strained inside the rock. Further, the clay swelling as a possible cause of permeability loss was discarded by injecting high salinity brine (3%) after the final fresh water flooding. No permeability restore appears there. The permeability behavior and the effluent fines concentration as function of PVI can be approximately reproduced by employing the data displayed in Table 3.

The model results are shown in Fig. 14 as blue solid lines and experimentally observed data as red circles. The fact that the first three salinity reduction steps yield no permeability loss nor fines production means that the fines maximum retention (critical) function, σ_{cr} , should be completely flat at these salinities ($C_s > 0.5$ wt. %), but further, in order to reproduce the observed behavior at even lower salinities ($C_s \leq 0.5$ wt. %), it should abruptly reduce. This is the general structure seen in the best adjusting function shown in Fig. 13(b). However, due to an extremely high sensitivity some very small variations occurring in σ_{cr} at $C_s > 0.5$ wt. % yield the unexpected k_{eff} reduction in that zone, Fig. 14(a). If we force σ_{cr} to exactly reproduce the flat zone of the intermediate salinities a deterioration of the permeability behavior at low salinity occurs. Anyway, by considering that data uncertainties are always present and are combined with the extremely high sensitivity mentioned above, we take the data matching as acceptable. The characteristic length of clogging is $\lambda_c^{-1} \sim 10$ m and detachment $\lambda_d^{-1} \sim 0.11$ m. Since $U \sim 1.32 \times 10^{-6}$ m/s the detachment characteristic time is $(U\lambda_d)^{-1} \sim 8.4 \times 10^4$ s, which corresponds to 3.3 PVI. This is a small time compare with the 100 PVI that the whole experiment lasts (see Fig. 14).

In their paper (Zeinijahromi et al., 2016) give the values $\sigma_{cr,0} = 0.0637$ and $\beta = 455$ for their tuning parameters. The dimensions they use is volumetric concentration. To transform these values to our

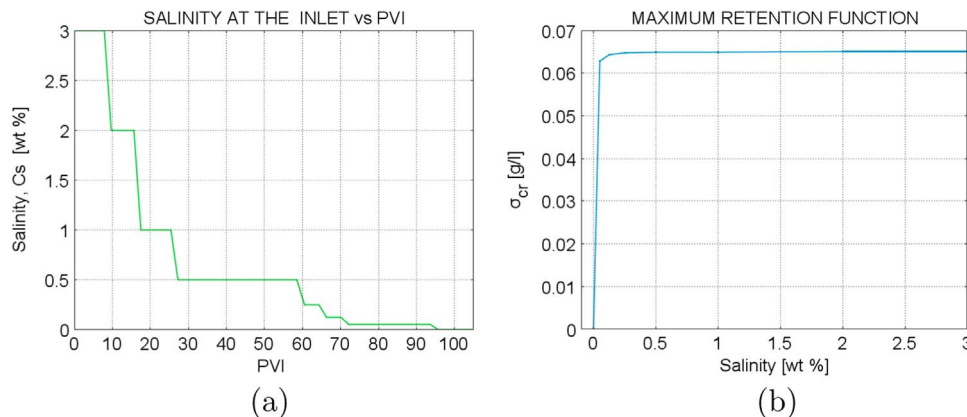


Fig. 13. Application to Zeinijahromi et al. data: (a) Salinity at inlet versus porous volume injected, and (b) Maximum retention function in terms of salinity.

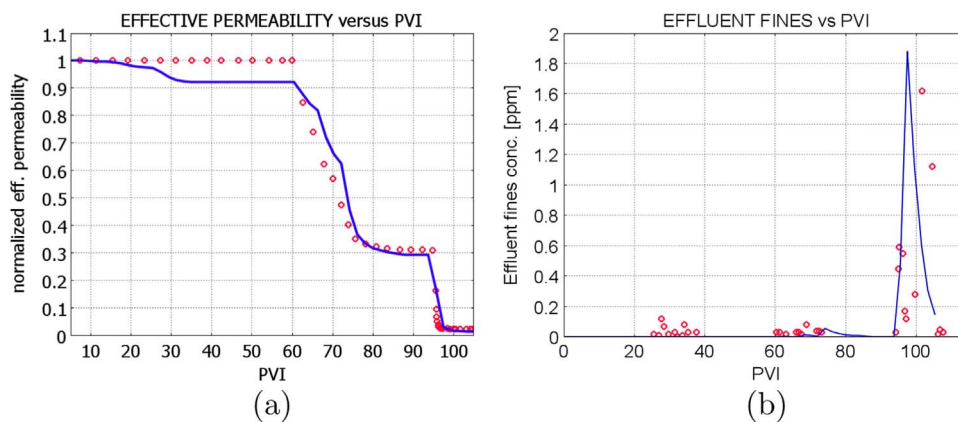


Fig. 14. [Color on-line] Reproduction of Zeinijahromi et al. data: (a) Permeability loss versus PVI, and (b) effluent fines concentration as function of PVI. Data points in red circles and model results as blue solid lines.

Table 3

Parameters used to reproduce the flooding data by Zeinijahromi et al. (2016).

Parameter	Value
Core length, L	17.0 cm
Core diameter, D	4.0 cm
Porosity, ϕ	20.0%
Porous volume, PV	42.7 ml
Initial permeability, k_0	76 mD
Water viscosity, μ	0.3 cP
Water density, ρ	1 g/ml
Total compressibility, c_T	6×10^{-10} 1/Pa
Longitudinal salt and mobile fines dispersivity, $\alpha_{L,s}$, $\alpha_{L,f}$	L/10
Injection rate, Q_{inj}	0.1 ml/min
Pressure at outlet, p_{out}	1015 psi
Rock fraction containing detachable fines, χ_f	8%w
Parameter $\sigma_{cr,0}$ in σ_{cr} (with $\sigma_{a0} = \sigma_{cr,0}$)	0.065 g/l
Detaching coefficient, λ_d	9 m^{-1}
Clogging coefficient, λ_c	0.1 m^{-1}
Formation damage coefficient, β	2.5×10^6 (g/l) $^{-1}$
Parameter nc in σ_{cr}	1.396
Parameter C_{s1} in σ_{cr}	0.00446 wt%
Parameter C_{s2} in σ_{cr}	-0.000847 wt%

dimensions the fines density is required, to which we take the clay density 1600 g/l. The values transform into $\sigma_{cr,0} = 3.98 \times 10^{-4}$ g/l (fines mass/rock volume) and $\beta = 7.28 \times 10^5$ l/g (rock volume/strained fines mass). These values are different from the values we obtained (see Table 3). The reason grounds probably in that different models for strained fines are used. We do not assume that all released particles get strained. Instead, we use Eq. (9) to describe the clogging fines dynamics and make use of the experimental effluent fines information. The difference becomes important since clogging fines play a crucial roll in the permeability loss.

Appendix A. The fitting method

In this Appendix we describe the procedure we developed to adjust our model to the experimental data of permeability loss, $k_{eff}(t)$, and effluent fines production, $C_f(z=L, t)$. Running the code demands relative large computing time, thus an adequate adjusting strategy is necessary. The procedure is general and can be applied to other models. It becomes more accurate as more known parameters are provided. In the three applications we described above we have fixed the parameters: porosity (ϕ), rock-fluid total compressibility (C_T), fluid viscosity (μ), fluid density (ρ), mass fraction content of detachable fines (clay content) (χ_f), injection rate (Q_{inj}), and dispersivities ($\alpha_{L,s}$ and $\alpha_{L,f}$). We have adjusted the parameters: detaching coefficient (λ_d), clogging coefficient (λ_c), formation damage, (β), and the parameters in the maximum retention function ($\sigma_{cr,0}$, nc , C_{s1} and C_{s2}). Some of these fitting parameters, such as λ_d and λ_c , can be experimentally evaluated, this will reduce the uncertainty in the parameter fitting result. Our adjusting procedure has the following sequence:

1. Perform a parameter sensitivity analysis to explore their impact on $k_{eff}(t)$ and $C_f(z=L, t)$. This provides information on the relevance that diverse

5. Concluding remarks

We have presented here an extended model to describe the permeability loss phenomenon due to fines migration and clogging, observed in single-phase laboratory core injection experiments. In the model we have introduced new elements with respect to previous published models. These new elements are (i) a modified kinetics for the adsorbed fines that smoothly brings the adsorbed fines concentration to the critical concentration, and (ii) an exponential expression for the attached fines maximum retention function, which has no divergence problems at small critical salinity concentration (CSC) values, and in the limiting case of relative large CSC it reproduces the expression frequently used before. The partial differential equation system is solved numerically, and the model is applied to data from three published laboratory single-phase core injection tests. A procedure to simultaneously adjust the model to the effective permeability history and the effluent fines concentration has been developed and employed. We conclude that our model reproduces adequately the experimentally observed behavior of the effective permeability loss and the effluent fines concentration. Additionally, the specific expression obtained for σ_{cr} from a given application could be used to link the experimental permeability loss results to microscopic detaching-attaching models.

Acknowledgements

The authors acknowledge support from the IMP projects D.61006 and D.61057 of the Gerencia de Ingeniería de Recuperación Adicional. They also thank an unknown journal reviewer for calling their attention on linking Eq. (7) to a deposition Langmuir blocking function.

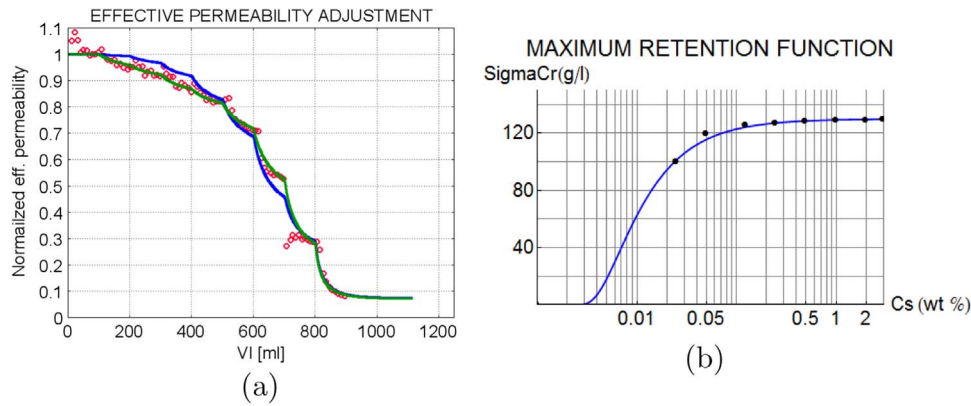


Fig. A.15. [Color on-line] Permeability adjustment of the Lever and Dawe case: (a) experimental data (red circles), point-by-point fitting (green line) and analytic function fitted (blue line), and (b) the corresponding maximum retention function in terms of salinity, point-by-point fitting (black dots) and best analytic function fitting (blue line).

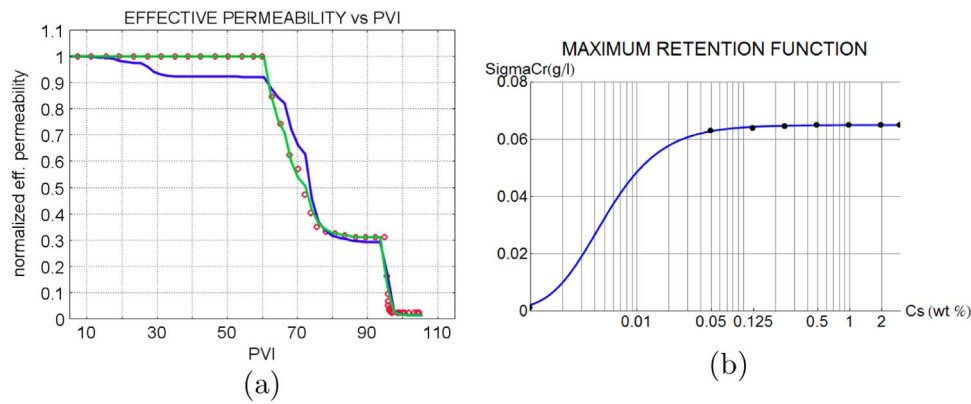


Fig. A.16. [Color on-line] Permeability adjustment of the Zeinijahromi et al. case: (a) experimental data (red circles), point-by-point fitting (green line) and analytic function fitted (blue line), and (b) the corresponding maximum retention function in terms of salinity, point-by-point fitting (black dots) and best analytic fitting (blue line).

- parameters will have on the data fitting, and the type of effect and uncertainty it induces. Specifically, in the three applications we have described, we found that ϕ , C_r , μ , ρ , Q_{inj} induce negligible effects; λ_d , λ_c , β and $\sigma_{cr,0}$ cause notorious effects, and nc , C_{s1} and C_{s2} have dramatic effects. Based on these results and the parameter type we defined the order and the way the parameters should be adjusted, as described below.
2. Use experimental information to fix the value of the parameters χ_f , λ_d , and λ_c . If not available, typical values should be chosen.
 3. Give a starting value for $\sigma_{cr,0}$, for example 75% of the $\sigma_{d0,max}$, and then adjust it to fit the maximum fine concentration peak height.
 4. Adjust β to reproduce the minimum value of k_{eff}/k_0
 5. If λ_d and λ_c were used as free parameters, then re-adjust them to fit the general permeability curve decay trend. Return to items (3) and (4) and continue to item (6).
 6. Adjust the permeability curve point-by-point at the times the salinity steps occur. Instead of directly fitting σ_{cr} by the analytical expression in Eq. (10), the point set $\{\sigma_{cr,i}, C_{s,i}\}$ should be used to temporarily fit k_{eff} , where $C_{s,i}$ is the salinity at step i with $i = 1, N$, been N the number of salinity reduction steps. This fitting procedure should always achieve an excellent permeability history matching. The resulting effluent fines production history matching should be acceptable, since its main peak value has been adjusted.
 7. Use the obtained point series $\{\sigma_{cr,i}, C_{s,i}\}$ to fit the analytical expression $\sigma_{cr}(C_s)$ of Eq. (10). This fitting can be done by a standard optimization procedure. We can weight the point data in order to give fitting preference to some specific salinity points. In our case we used Nelder-Mead as implemented in *Mathematica*. At the end we obtain the best three parameters nc , C_{s1} and C_{s2} . The cases where the experimental k_{eff} data show no loss at the initial salinity reduction steps are particularly hard to describe by $\sigma_{cr}(C_s)$, however good approximations could be achieved, as shown in the plots of the applications, Figs. (10), (12), (14).

To illustrate the procedure we present Figs. (A.15) and (A.16), where the effective permeability is shown in plot (a) and the corresponding maximum retention function in a semi-log plot in (b). In (a) the experimental data points, the point-by-point data fitting (green curve) and the final analytic function fitting (blue curve) are displayed. In (b) the points corresponding to the point-by-point fitting and the best $\sigma_{cr}(C_s)$ matching analytical function are plotted.

It is to be noticed in (Fig. A.16(b)) that extremely small differences between the analytical expression $\sigma_{cr}(C_s)$ (blue curve) and the exact fitting points (black dots), particularly at high salinities, can give place to important differences in the permeability (Fig. A.16(a)).

References

- Adamczyk, Z., 2003. Particle adsorption and deposition: role of electrostatic interactions. *Adv. Colloid Interface Sci.* 100–102, 267–347.
- Al-Shalabi, E.W., Sepehrnoori, K., 2016. A comprehensive review of low salinity/engineered water injections and their applications in sandstone and carbonate rocks. *J. Pet. Sci. Eng.* 139, 137–161.
- Bedrikovetsky, P., Siqueira, F.D., Furtado, C.A., Souza, A.L.S., 2010. Modified particle detachment model for colloidal transport in porous media. *Transp. Porous Media* 86 (2), 353–383.
- Chen, Z., Huan, G., Ma, Y., 2006. *Computational Methods for Multiphase Flows in Porous Media*. SIAM, Philadelphia.
- Civan, F., 2016. Modified formulations of particle deposition and removal kinetics in saturated porous media. *Transp. Porous Media* 111 (2), 381–410.
- Comsol, 2008. *COMSOL Multiphysics: Version 3.5a. User's guide*.
- Fogden, A., Kumar, M., Morrow, N.R., Buckley, J.S., 2011. Mobilization of fine particles during flooding of sandstones and possible relations to enhanced oil recovery. *Energy Fuels* 25 (4), 1605–1616.
- Hussain, F., Zeinijahromi, A., Bedrikovetsky, P., Badalyan, A., Carageorgos, T., Cinar, Y., 2013. An experimental study of improved oil recovery through fines-assisted waterflooding. *J. Pet. Sci. Eng.* 109, 187–197.
- Khilar, K., Fogler, H., 1984. The existence of a critical salt concentration for particle release. *J. Colloid Interface Sci.* 101 (1), 214–224.
- Khilar, K., 1981. *The Water Sensitivity of Berea Sandstones*. (Ph.D. thesis). University of Michigan.
- Lever, A., Dawe, R.A., 1984. Water-sensitivity and migration of fines in the hopeman sandstone. *J. Pet. Geol.* 7 (1), 97–107.
- Logan, J.D., 2001. *Transport Modeling in Hydrogeochemical Systems*. Springer-Verlag, New York.
- Oliveira, M.A., Vaz, A.S., Siqueira, F.D., Yang, Y., You, Z., Bedrikovetsky, P., 2014. Slow migration of mobilised fines during flow in reservoir rocks: laboratory study. *J. Pet. Sci. Eng.* 122, 534–541.
- Pang, S., Sharma, M., 1997. A model for predicting injectivity decline in water-injection wells. *SPE Formation Evaluation* (September), 194–201, sPE 28489.
- Sarkar, A., Sharma, M., 1990. Fines migration in two-phase flow. *Journal of Petroleum Technology* (May), 646–652, sPE 17437.
- Sheng, J., 2014. Critical review of low-salinity waterflooding. *J. Pet. Sci. Eng.* 120, 216–224.
- Wennberg, K., Batrouni, G., A., H., 1995. Modelling fines mobilization, migration and clogging. In: *Proceedings of European Formation Damage Conference Held in The Hague, The Netherlands*. 15–16 May, 1995. SPE 30111.
- Zeinijahromi, A., Vaz, A., Bedrikovetsky, P., Borazjani, S., 2012. Effects of fines migration on well productivity during steady state production. *J. Porous Media* 15 (7), 665–679.
- Zeinijahromi, A., Farajzadeh, R., Bruining, J., Bedrikovetsky, P., 2016. Effect of fines migration on oil-water relative permeability during two-phase flow in porous media. *Fuel* 176, 222–236.
- Zeinijahromi, A., Bedrikovetsky, P., 2013. Physics mechanisms of enhanced recovery by fines-migration-assisted waterflooding (laboratory study). In: *SPE European Formation Damage Conference and Exhibition, Noowijk, The Netherlands*. 5–7 June, 2013, SPE 165190.